Bulletin of the Earthquake
Research Institute
Vol. 42 (1964), pp. 369-381

17. *Tsunami in the Vicinity of a Wave Origin* [II].

By Takao Momoi,

Earthquake Research Institute.

(Read March 24, 1964.—Received March 31, 1964.)

Abstract

This work is the continuation of the previous study on the generation of a tsunami in the near field for a three-dimensional case, which has been done by means of numerical calculation resorting to an electronic computer. The method of analysis follows nearly the same line as that in the previous paper of the same title. Such a method, with a little modification, makes it possible to compute further the wave height of a tsunami in the near field, even though it is very low in efficiency.

According to the results of the computation, it turns out that: (1) the variation of waves at the central part is more rapid than in other parts: (2) as far as the later phase is concerned, at the central part of the wave origin and only in this part, the motion of the waves goes above the mean level of water. In other words, in the parts excluding the center the undulations are superposed on the tail of the long wave.

From the second reason described above, the approximation of the shallow water seems to be still in use for the analysis of the phenomena in the present stage ($t^*=21\sim45$).

1. Introduction

In the preceding paper[1], the author calculated the wave heights of the tsunami at nearby points occupying the wave origin. Then, as t^* (time variable) increases, the method of computations prevents us proceeding with the integration, which is due mainly to the existence of the vibrating factor $\cos \omega^* t^*$ included in the expression of the wave height (see the formal expression (1) in section 2). Although the method of integration used in the previous study is inadvisible from the point of view of cost and efficiency, the main part of the work in this paper follows almost the same lines as that of paper I.

1) T. Momoi, *Bull. Earthq. Res. Inst.*, **42** (1964), 133. This paper will be referred to as paper I in the following discussions.

2. Method of Analysis

In calculation, the crux of the problem is the avoidance of the difficulty of integration due to the time factor $\cos\omega^*t^*$. As described in the introduction, the entire portion of the present study is worked out in a very similar way to the previous one. Though the efficiency is low, for the present stage ($t^*=21\sim45$) of the computation, the method of the previous analysis is still applicable with a little modification.

For reference, the formal expression of the wave height produced by an instantaneous elevation of a portion of the sea bottom within a radius a^* is given below:

$$\zeta_R=a^*\int_0^\infty \frac{\cos\omega^*t^*}{\cosh k^*}J_0(k^*r^*)J_1(k^*a^*)dk^* \ , \tag{1}$$

where the notations and definitions are exactly the same as in the preceding paper I.

When a time parameter t^* becomes large, the value of ω^*t^* ($\omega^*=\sqrt{k^*\tanh k^*}$) varies remarkably even for a very small increment Δk^*. But such rapid variation takes place mainly in the range of a small k^*, where a gradient of ω^* is greater in magnitude than in the range of a large k^*. It may be surmised from the curve of $\omega^*=\sqrt{k^*\tanh k^*}$ in Fig. 1. Whereas no discussion for $J_0(k^*r^*)$ including a position parameter r^* has been made so far. For the range of $r^*=0\sim27.5$, if a number of divisions of the integration is taken, such as a divided interval less than that of the previous work[1], the integration (1) is expected *at least* to have the same accuracy as in paper I. These circumstances limit our

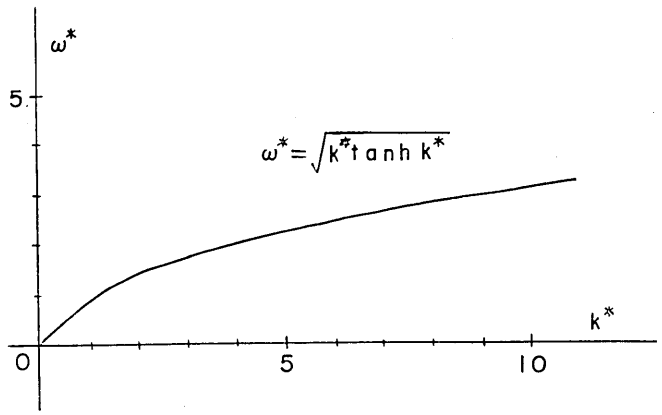

Fig. 1.

attention only to a consideration of the former problem in this paragraph, i.e., with regard to the time parameter t^*.

As previously noted, the rapid variation of $\cos \omega^* t^*$ is due mainly to the large gradient of ω^* in the lower range of k^*. If we change the divided intervals of the integration so as to fit the *gradient* of the relevant part of ω^*, a number of the divisions of the integration in the lower part of k^* is forced to be greater than in the upper part. This process is propounded in the following.

As in paper I, the parameter a^* is specified as 10 in the present study. Hence, if the interval of the integration (1) is limited to the range $k^*=0\sim10$, the error from the cut-off integration behaves like that in the previous work[1]. Then a simple way to make the variation of $\cos \omega^* t^*$ slight seems to be by the following procedure. The interval (0, 10) is separated into ten regions, i.e., (0, 1), (1, 2), (2, 3), ---, (8, 9), (9, 10). In the n-th region (n-1, n), a number of the divisions of the integration should be taken in proportion to the average gradient of ω^* in the relevant interval, which might approximately be given by the relation

$$\omega_n^* - \omega_{n-1}^* \propto N_n \,, \qquad (2)$$

where (refer to Fig. 2)

ω_{n-1}^* and ω_n^* : the values of ω^* at $k^*=n$-1 and n;

N_n : the number of the divisions in the n-th interval.

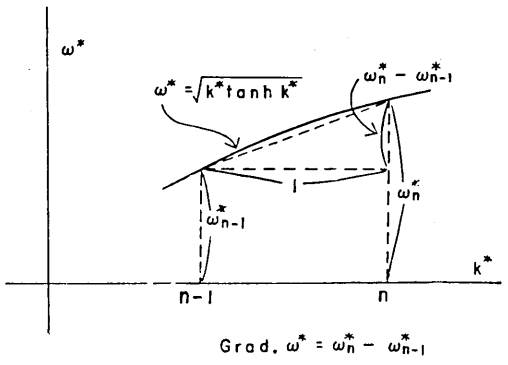

Fig. 2. A gradient of ω^* in the n-th interval.

The values of ω^* for k^* (=0, 0.5, ---, 10) are tabulated in Table 1, of which the curve is plotted in Fig. 1. Using these values, N_n is computed essentially in accordance with the formula (2). To determine the proportionality coefficient of the expression (2), we need one more requirement that the divided intervals of the integration be less than those in paper I to make the integration converge for the position parameter r^*. For the value of 0.04, such a requirement is approximately satisfied. The choice of the above value leads to the determination of N_n values at each interval, as shown in Table 2. In the present study, since the method of the integration follows Simpson's rule, N_n must consist of even numbers. Therefore, N_n values computed by the relation (2) are

Table 1. The values of ω^* versus a variable k^*.

k^*	ω^*	k^*	ω^*
0.0	0.0000000	5.5	0.2345168×10^{1}
0.5	0.4806855×10^{0}	6.0	0.2449474×10^{1}
1.0	0.8726936×10^{0}	5.5	0.2549503×10^{1}
1.5	0.1165213×10^{1}	7.0	0.2645749×10^{1}
2.0	0.1388544×10^{1}	7.5	0.2738611×10^{1}
2.5	0.1570520×10^{1}	8.0	0.2828426×10^{1}
3.0	0.1727762×10^{1}	8.5	0.2915475×10^{1}
3.5	0.1869123×10^{1}	9.0	0.2999999×10^{1}
4.0	0.1999329×10^{1}	9.5	0.3082206×10^{1}
4.5	0.2121058×10^{1}	10.0	0.3162277×10^{1}
5.0	0.2235966×10^{1}		

Table 2. Numbers of the divisions at each interval.

k^*	N_n	k^*	N_n
0~1	174	5~ 6	42
1~2	104	6~ 7	40
2~3	68	7~ 8	36
3~4	54	8~ 9	34
4~5	48	9~10	32

rounded so as to consist of even numbers. Now applying Simpson's formula to each interval $((n\text{-}1)\sim n)$ with a relevant number (N_n) of the divisions, the numerical integrations are carried out with the use of the electronic computer.

3. Computation and Discussion

The computed results are tabulated in Table 3 and graphically shown in Fig. 3. The calculations are made for the range $t^*=21\sim45$ up to 27.5 with regard to the position parameter r^*.

In order to check the convergence of the integration, the number of the divisions at each interval is doubled, the results of which are given in Table 4 only for the case of $t^*=45$. Since the variation of $\cos\omega^*t^*$ is rather gradual for t^* of less than 45, to make the calculation only for the case of $t^*=45$ suffices for an examination of the convergence of the integration for other t^*. In comparison with Table 4, the values tabulated in Table 3 are found to have an accuracy of at least three decimal digits.

In drawing the graphs, the scales of the ordinates are appropriately changed allowing for a relative smallness of the wave heights, in the stages ($t^*=21\sim45$) of the present work, as compared with those in paper I, so that the figures enable us to visualize the minute variations of the wave heights in the later phase. In Figs. 3a and 3b, the ordinates

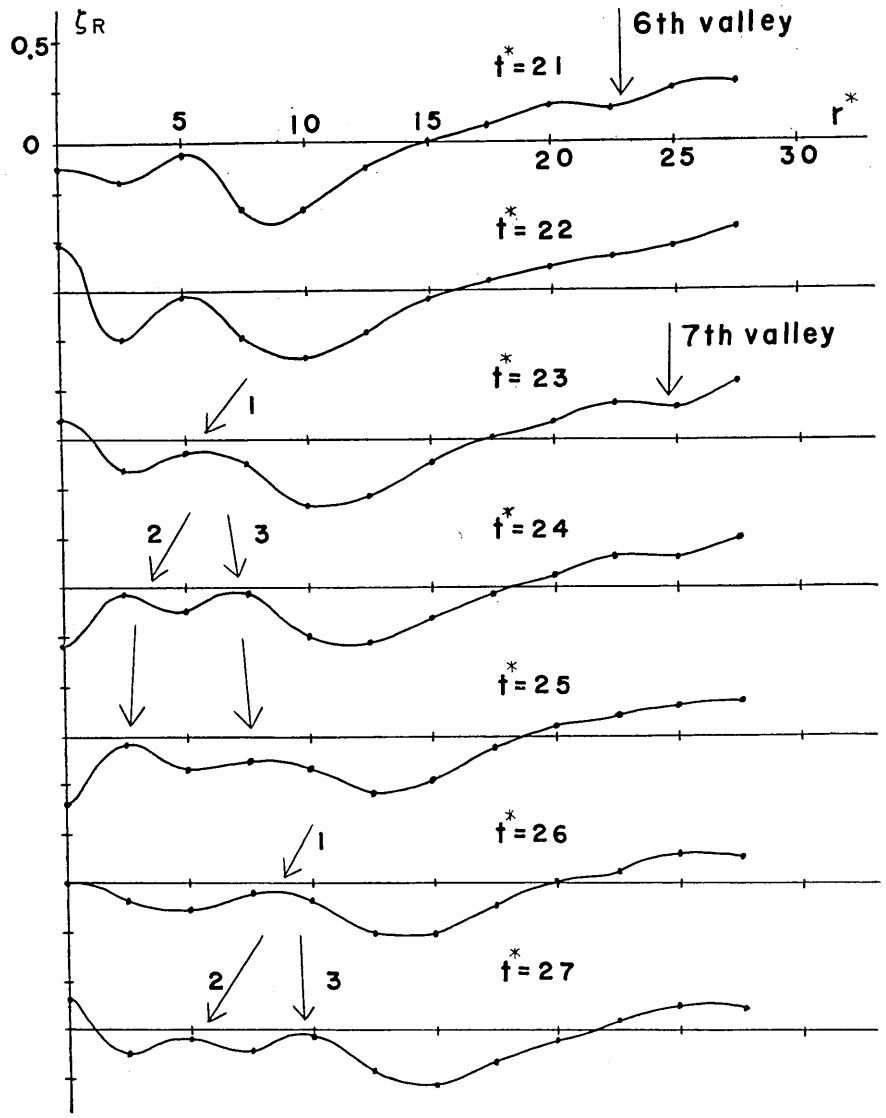

Fig. 3a.

are in scale unit twice those of the previous paper, while, in Figs. 3c and 3d, they are scaled up four times.

As we pass from the first ($t^*=21$) to the seventh figures ($t^*=27$) in Fig. 3a, the continuation of the small valleys discussed in the previous work is seen near the tops of the first crests, which are designated by

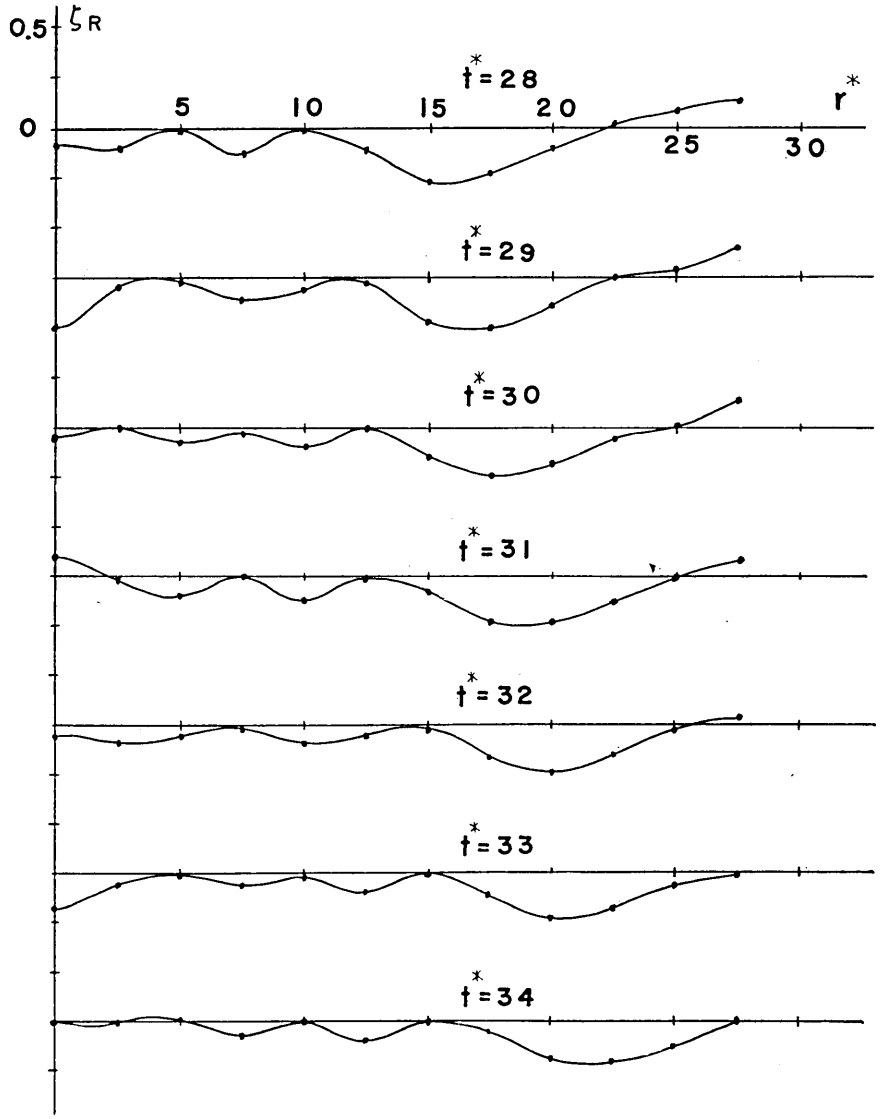

Fig. 3b.

"6th valley" and "7th valley" in the figures. They are propagated backwards as described in paper I.

In this purview, the discussion will be mainly focussed upon the phenomena of the later phase.

According to the theory based on the long wave approximation, a

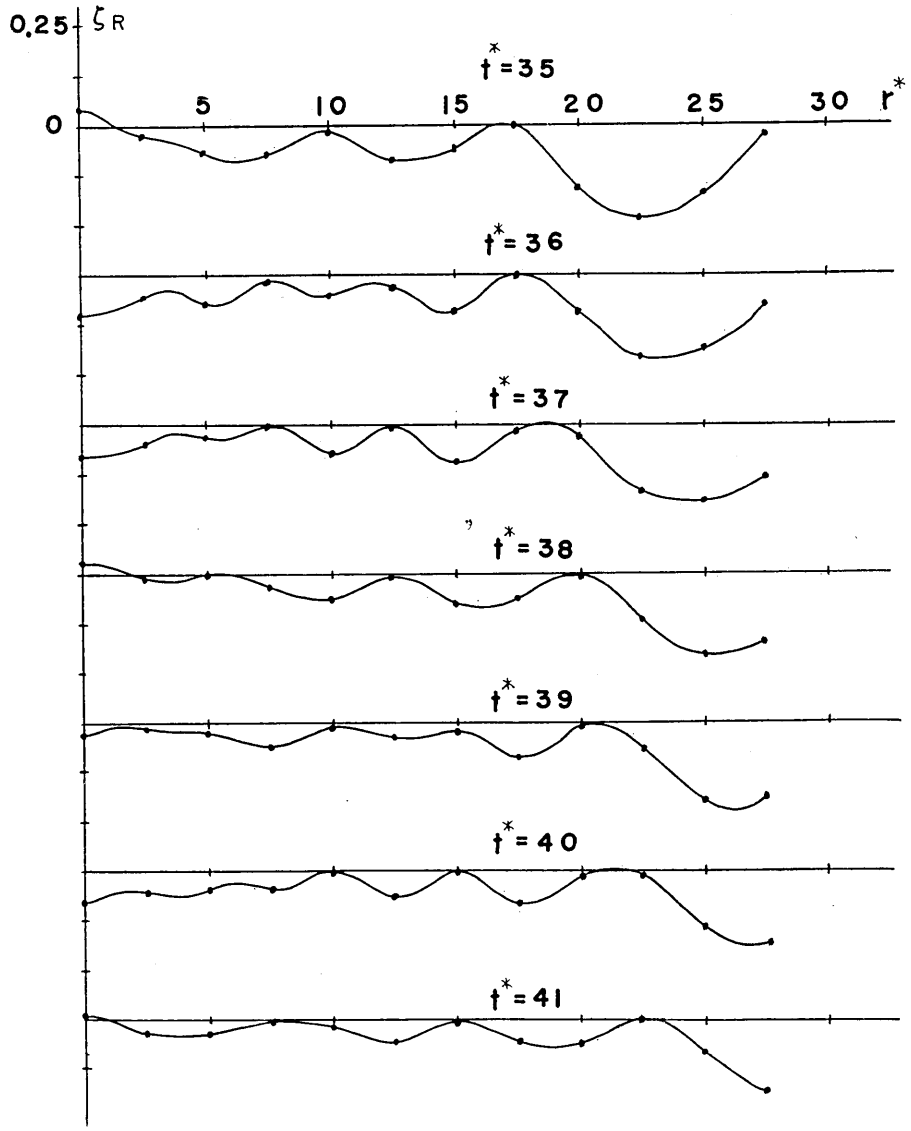

Fig. 3c.

very sharp valley and only one appears in a part of the later phase, which is followed by a long tail gradually approaching to the mean level of the water from below. According to the results of the numerical calculation, however, the small valleys subsequently appear after the first large valley. These small valleys prevail throughout all the figures.

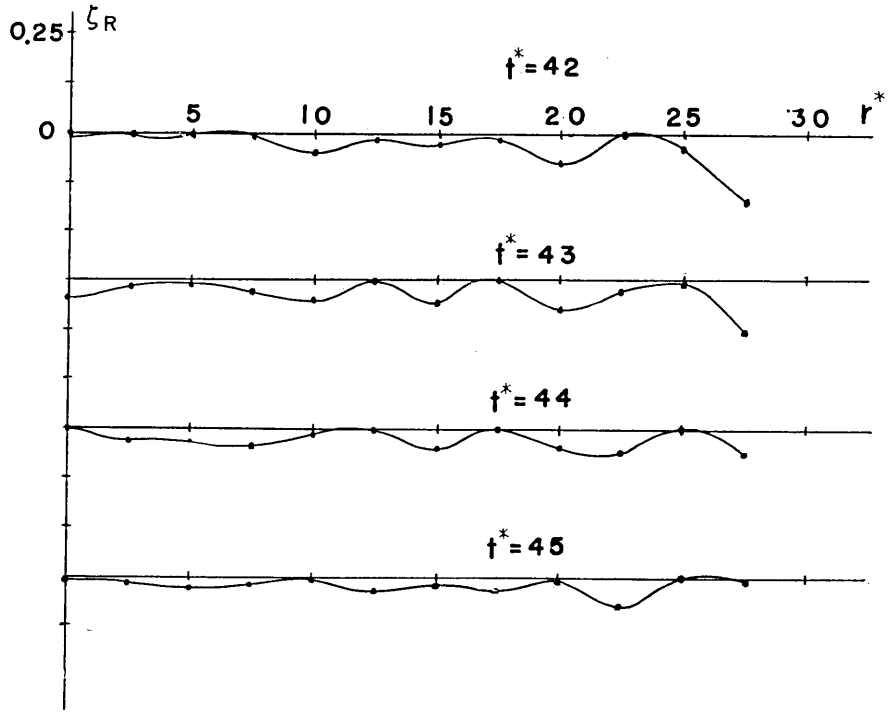

Fig. 3d.

In the center (the exact point) of the wave origin, the surface of the water moves up and down through the mean level of the sea, and, as far as the later phase is concerned, only in this part does the water surface go above the mean level. The motion in this central part proceeds rather quickly than in other part. Such a rapid motion is considered to be due to the convergence of the retrogressive waves, which will be explained in the next.

Referring to the figures designated by the parameters $t^*=23$ to 26 and 26 to 29, the second crest (with a stated number "1") is generated after the first large valley is separated into two crests (with "2" and "3"), one of which is progressive and the other retrogressive. The former disappears into the first largest valley, while the latter being

Table 3. The variation of the tsunami heights in the near field versus time.

r^*	ζ_R ($t^*=21$)	ζ_R ($t^*=22$)	ζ_R ($t^*=23$)
0.0	-0.1337969×10^{0}	0.2425994×10^{0}	0.9047025×10^{-1}
2.5	-0.2171539×10^{0}	-0.2676409×10^{0}	-0.1537128×10^{0}
5.0	-0.6283778×10^{-1}	-0.1655659×10^{-1}	-0.6378861×10^{-1}
7.5	-0.3495427×10^{0}	-0.2384424×10^{0}	-0.1177961×10^{0}
10.0	-0.3475829×10^{0}	-0.3663542×10^{0}	-0.3411538×10^{0}
12.5	-0.1645390×10^{0}	-0.2280038×10^{0}	-0.2826078×10^{0}
15.0	-0.6969858×10^{-2}	-0.6158100×10^{-1}	-0.1170065×10^{0}
17.5	0.9951638×10^{-1}	0.6425843×10^{-1}	0.6381168×10^{-2}
20.0	0.1723091×10^{0}	0.1148641×10^{0}	0.7518296×10^{-1}
22.5	0.1552041×10^{0}	0.1703888×10^{0}	0.1826137×10^{0}
25.0	0.2691446×10^{0}	0.2043192×10^{0}	0.1533254×10^{0}
27.5	0.2893070×10^{0}	0.3089425×10^{0}	0.2910798×10^{0}

r^*	ζ_R ($t^*=24$)	ζ_R ($t^*=25$)	ζ_R ($t^*=26$)
0.0	-0.3126623×10^{0}	-0.3485438×10^{0}	0.9296316×10^{-2}
2.5	-0.3788366×10^{-1}	-0.2513627×10^{-1}	-0.7332868×10^{-1}
5.0	-0.1459898×10^{0}	-0.1815262×10^{0}	-0.1410569×10^{0}
7.5	-0.3267816×10^{-1}	-0.1471913×10^{-1}	-0.5936261×10^{-1}
10.0	-0.2713835×10^{0}	-0.1728067×10^{0}	-0.7619971×10^{-1}
12.5	-0.3169368×10^{0}	-0.3194534×10^{0}	-0.2834407×10^{0}
15.0	-0.1732308×10^{0}	-0.2283573×10^{0}	-0.2701731×10^{0}
17.5	-0.3730086×10^{-1}	-0.7175380×10^{-1}	-0.1259634×10^{0}
20.0	0.6589615×10^{-1}	0.5186336×10^{-1}	0.3196321×10^{-2}
22.5	0.1592555×10^{0}	0.1048468×10^{0}	0.5562752×10^{-1}
25.0	0.1379128×10^{0}	0.1517606×10^{0}	0.1637200×10^{0}
27.5	0.2410817×10^{0}	0.1800914×10^{0}	0.1354788×10^{0}

r^*	ζ_R ($t^*=27$)	ζ_R ($t^*=28$)	ζ_R ($t^*=29$)
0.0	0.1663739×10^{0}	-0.9851518×10^{-1}	-0.2714464×10^{0}
2.5	-0.1194960×10^{0}	-0.1203583×10^{0}	-0.5585501×10^{-1}
5.0	-0.5871657×10^{-1}	-0.1103204×10^{-1}	-0.3671024×10^{-1}
7.5	-0.1233904×10^{0}	-0.1517322×10^{0}	-0.1190926×10^{0}
10.0	-0.1620571×10^{-1}	-0.1300842×10^{-1}	-0.5722848×10^{-1}
12.5	-0.2126634×10^{0}	-0.1244780×10^{0}	-0.4653144×10^{-1}
15.0	-0.2903069×10^{0}	-0.2798562×10^{0}	-0.2356708×10^{0}
17.5	-0.1873981×10^{0}	-0.2282421×10^{0}	-0.2540578×10^{0}
20.0	-0.6003368×10^{-1}	-0.1032027×10^{0}	-0.1338886×10^{0}
22.5	0.3610758×10^{-1}	0.2829955×10^{-1}	0.4330094×10^{-2}
25.0	0.1442749×10^{0}	0.9337135×10^{-1}	0.4046186×10^{-1}
27.5	0.1236156×10^{0}	0.1368200×10^{0}	0.1472949×10^{0}

(to be continued)

(continued)

r^*	ζ_R $(t^*=30)$	ζ_R $(t^*=31)$	ζ_R $(t^*=32)$
0.0	-0.5096617×10^{-1}	0.1129578×10^{0}	-0.7217172×10^{-1}
2.5	-0.5109874×10^{-2}	-0.4829511×10^{-1}	-0.1004548×10^{0}
5.0	-0.9362873×10^{-1}	-0.1081836×10^{0}	-0.6152487×10^{-1}
7.5	-0.5248258×10^{-1}	-0.9198347×10^{-2}	-0.2333786×10^{-1}
10.0	-0.1112924×10^{0}	-0.1320538×10^{0}	-0.1020881×10^{0}
12.5	-0.5805500×10^{-2}	-0.1392408×10^{-1}	-0.5766893×10^{-1}
15.0	-0.1654758×10^{0}	-0.8724924×10^{-1}	-0.2544586×10^{-1}
17.5	-0.2665398×10^{0}	-0.2454385×10^{0}	-0.1928833×10^{0}
20.0	-0.1804128×10^{0}	-0.2313168×10^{0}	-0.2499663×10^{0}
22.5	-0.6663251×10^{-1}	-0.1252452×10^{0}	-0.1570843×10^{0}
25.0	0.1262506×10^{-1}	0.3583641×10^{-2}	-0.1877657×10^{-1}
27.5	0.1289519×10^{0}	0.8034148×10^{-1}	0.2627287×10^{-1}

r^*	ζ_R $(t^*=33)$	ζ_R $(t^*=34)$	ζ_R $(t^*=35)$
0.0	-0.1826739×10^{0}	-0.3342451×10^{-2}	0.4949715×10^{-1}
2.5	-0.6571266×10^{-1}	-0.1321041×10^{-1}	-0.2536150×10^{-1}
5.0	-0.1289667×10^{-1}	-0.2075211×10^{-1}	-0.6431852×10^{-1}
7.5	-0.7102185×10^{-1}	-0.9461016×10^{-1}	-0.6600041×10^{-1}
10.0	-0.4483471×10^{-1}	-0.6589406×10^{-2}	-0.1604417×10^{-1}
12.5	-0.1035193×10^{0}	-0.1173306×10^{0}	-0.8805177×10^{-1}
15.0	-0.2401558×10^{-3}	-0.1674311×10^{-1}	-0.5935271×10^{-1}
17.5	-0.1270642×10^{0}	-0.5900894×10^{-1}	-0.9982094×10^{-2}
20.0	-0.2349880×10^{0}	-0.2079261×10^{0}	-0.1636161×10^{0}
22.5	-0.1794838×10^{0}	-0.2131345×10^{0}	-0.2387550×10^{0}
25.0	-0.7195002×10^{-1}	-0.1351630×10^{0}	-0.1752818×10^{0}
27.5	-0.6823179×10^{-2}	-0.1875425×10^{-1}	-0.3573170×10^{-1}

r^*	ζ_R $(t^*=36)$	ζ_R $(t^*=37)$	ζ_R $(t^*=38)$
0.0	-0.1053493×10^{0}	-0.8338378×10^{-1}	0.3242543×10^{-1}
2.5	-0.6426967×10^{-1}	-0.5753012×10^{-1}	-0.1795998×10^{-1}
5.0	-0.7487107×10^{-1}	-0.3668207×10^{-1}	-0.8182507×10^{-2}
7.5	-0.1886592×10^{-1}	-0.7797699×10^{-2}	-0.4008359×10^{-1}
10.0	-0.5692642×10^{-1}	-0.8311557×10^{-1}	-0.6559731×10^{-1}
12.5	-0.3732764×10^{-1}	-0.3871250×10^{-2}	-0.1157965×10^{-1}
15.0	-0.9805191×10^{-1}	-0.1055529×10^{0}	-0.7587938×10^{-1}
17.5	0.1548593×10^{-2}	-0.2095195×10^{-1}	-0.6164467×10^{-1}
20.0	-0.9495846×10^{-1}	-0.3194665×10^{-1}	-0.2122918×10^{-2}
22.5	-0.2234319×10^{0}	-0.1733566×10^{0}	-0.1207580×10^{0}
25.0	-0.1885223×10^{0}	-0.1984186×10^{0}	-0.2123742×10^{0}
27.5	-0.7958531×10^{-1}	-0.1400777×10^{0}	-0.1848554×10^{0}

(to be continued)

(continued)

r^*	ζ_R $(t^*=39)$	ζ_R $(t^*=40)$	ζ_R $(t^*=41)$
0.0	-0.3789326×10^{-1}	-0.7989278×10^{-1}	0.1276993×10^{-2}
2.5	-0.1965230×10^{-1}	-0.5008691×10^{-1}	-0.4069672×10^{-1}
5.0	-0.2876131×10^{-1}	-0.5716922×10^{-1}	-0.4308245×10^{-1}
7.5	-0.6713784×10^{-1}	-0.5038433×10^{-1}	-0.1396610×10^{-1}
10.0	-0.2359828×10^{-1}	-0.3167054×10^{-2}	-0.2376004×10^{-1}
12.5	-0.4784421×10^{-1}	-0.7424293×10^{-1}	-0.6324940×10^{-1}
15.0	-0.2998668×10^{-1}	-0.1222291×10^{-2}	-0.9036628×10^{-2}
17.5	-0.9387075×10^{-1}	-0.9522665×10^{-1}	-0.6501327×10^{-1}
20.0	-0.9765953×10^{-3}	-0.2408218×10^{-1}	-0.6436562×10^{-1}
22.5	-0.7325856×10^{-1}	-0.2298520×10^{-1}	0.1035888×10^{-1}
25.0	-0.2046250×10^{-1}	-0.1560281×10^{0}	-0.8896980×10^{-1}
27.5	-0.1966887×10^{0}	-0.1903089×10^{0}	-0.1857099×10^{0}

r^*	ζ_R $(t^*=42)$	ζ_R $(t^*=43)$	ζ_R $(t^*=44)$
0.0	-0.2071932×10^{-1}	-0.5555909×10^{-1}	-0.9575868×10^{-2}
2.5	-0.1443164×10^{-1}	-0.2458035×10^{-1}	-0.4018033×10^{-1}
5.0	-0.1203388×10^{-1}	-0.1674241×10^{-1}	-0.4197536×10^{-1}
7.5	-0.8642462×10^{-2}	-0.3687935×10^{-1}	-0.5086247×10^{-1}
10.0	-0.5505289×10^{-1}	-0.5502734×10^{-1}	-0.2388210×10^{-1}
12.5	-0.2618714×10^{-1}	-0.1648510×10^{-2}	-0.1349646×10^{-1}
15.0	-0.4209879×10^{-1}	-0.6737441×10^{-1}	-0.5998985×10^{-1}
17.5	-0.2311560×10^{-1}	0.1165126×10^{-2}	-0.7630058×10^{-2}
20.0	-0.9117022×10^{-1}	-0.8497107×10^{-1}	-0.5483353×10^{-1}
22.5	0.6163059×10^{-3}	-0.3664756×10^{-1}	-0.6728383×10^{-1}
25.0	-0.3961341×10^{-1}	-0.1348417×10^{-1}	0.2098552×10^{-2}
27.5	-0.1757287×10^{0}	-0.1372471×10^{0}	-0.7216884×10^{-1}

r^*	ζ_R $(t^*=45)$
0.0	-0.2454479×10^{-1}
2.5	-0.2390638×10^{-1}
5.0	-0.3697378×10^{-1}
7.5	-0.2809909×10^{-1}
10.0	-0.3038057×10^{-2}
12.5	-0.4387479×10^{-1}
15.0	-0.2714107×10^{-1}
17.5	-0.3848310×10^{-1}
20.0	-0.1733665×10^{-1}
22.5	-0.8205269×10^{-1}
25.0	-0.2331027×10^{-3}
27.5	-0.1564376×10^{-1}

propagated inside induces the rapid variation of the water surface at the center of the wave origin. In a like manner, such phenomena seem to be seen in other figures, but the correspondence of the small crests between the figures are far from certain. Hence, the further remark to account for these phenomena is suggested to the readers.

Table 4. The results of the integration made under a doubled number of the divisions.

r^*	ζ_R $(t^*=45)$	r^*	ζ_R $(t^*=45)$	r^*	ζ_R $(t^*=45)$
0.0	-0.2457459×10^{-1}	10.0	-0.3062846×10^{-2}	20.0	-0.1736419×10^{-1}
2.5	-0.2392014×10^{-1}	12.5	-0.4389397×10^{-1}	22.5	-0.8205614×10^{-1}
5.0	-0.3698774×10^{-1}	15.0	-0.2715306×10^{-1}	25.0	-0.2486058×10^{-3}
7.5	-0.2811813×10^{-1}	17.5	-0.3849825×10^{-1}	27.5	-0.1567166×10^{-1}

Looking through all the figures, one of the most outstanding features is that the undulations of the later phase, except for the movement at the central part, take place below the mean level of the water. In the preceding paper I, we came to the conclusion that the tsunami, in the initial stage, markedly resembles in shape that derived from the theory based on the long wave approximation. This fact seems to be valid for the tsunami of the later phase in the present stage, which is explained with the help of the figure (Fig. 4).

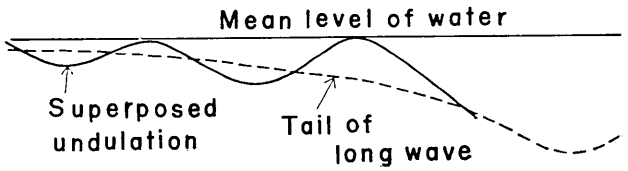

Fig. 4.

In Fig. 4, the broken line stands for a schematical line of the long wave and the bold line the small undulation superposed on the hypothetical tail of the long wave. As shown in the figure, if we assume that the waves in the later phase (in Fig. 3) as consisting of two kinds of waves with different wave numbers, i.e., the one being the long wave and the other the waves of the large wave numbers, the behavior of the later phase below the free surface of water would be satisfactorily explained.

17. 波源域における津波 [II]

地震研究所 桃 井 高 夫

本報告は，波源域における津波を電子計算機を用いて解明した前報告の続きであり，前報告では，第1波の変化を主に論じたのに対し，本報告では，第2波以下 (later phase) の波について，数値解析をおこなつた．数値解析の方法は，前報告で用いたのとほぼ同じで，積分するときの分割方法を少し変えただけである．

計算結果によれば，

(1) 波源域の丁度中心における津波の変化は他の部分の変化に比べて早く進行する．

(2) 第2波以下 (later phase) の波について，中心地域を除けば，すべて平均水面（ここでは，海底変化のおこる以前の海面を意味する）より下側で振動している，ことが分つた．

上記の第2の現象は，長波近似によつて得られる長波 (long wave) の上に波長の短い波が，重つたと解釈すれば，前報告で出した，津波発生の初期では長波近似がよくあてはまるという結論が，本報告の later phase についてもいえることが分かる．